

The return of nucleon strangeness?

T. J. Hobbs¹, Mary Alberg^{1,2}, Gerald A. Miller¹

¹*Department of Physics, University of Washington, Seattle, Washington 98195, USA*

²*Department of Physics, Seattle University, Seattle, Washington 98122, USA*

(Dated: January 27, 2023)

Determining the nonperturbative $s\bar{s}$ content of the nucleon has attracted considerable interest and been the subject of numerous experimental searches. These measurements used a variety of reactions and place important limits on the vector form factors observed in parity-violating PV elastic scattering and the parton distributions of deep inelastic scattering, DIS. In spite of this progress, attempts to relate information obtained from elastic and DIS experiments have been sparse. To ameliorate this situation, we develop an interpolating model using light-front wave functions capable of computing both DIS and elastic observables. This framework is used to show that existing knowledge of DIS places significant restrictions on our wave function. The result is that the predicted effects of nucleon strangeness on elastic observables is much smaller than those tolerated by direct fits to PV elastic scattering data alone. In particular, we find the narrow limits $-0.024 \leq \mu_s \leq 0.035$, and $-0.137 \leq \rho_s^D \leq 0.081$ for the strange contributions to the nucleon magnetic moment and charge radius using our model, which are about ten times smaller than previous bounds.

I. INTRODUCTION

A precise understanding of the nonperturbative structure of the nucleon remains an elusive goal half a century since the advent of the quark model [1, 2]. Following the revelation of the “proton spin crisis” by the EMC collaboration [3], the desire to map the internal landscape of the nucleon has driven many experimental efforts to discover the origin of its flavor and spin content.

In this respect, parity-violating (PV) lepton-nucleon experiments have shed considerable light by merit of their sensitivity to the flavor structure of various quark currents within the struck nucleon, with elastic and deeply inelastic scattering (DIS) measurements providing complementary information. For the former, reactions of the type $eN \rightarrow e'N'$ are capable of discriminating the quark-level contributions to the charge, magnetization, and axial structure of the nucleon, whereas the DIS mechanism $eN \rightarrow e'X$ enables the extraction of the probabilistic quark or parton distribution functions (PDFs).

The properties of QCD suggest that matrix elements of the nucleon involving strange quarks should in general be non-zero, and as such must be associated with some nonperturbative “strangeness” content of the nucleon which would have observable consequences for elastic form factors [4]. This recognition spurred multiple efforts (See Ref. [5] for a recent review) to detect the signatures for nucleon strangeness in PV elastic measurements at SAMPLE [6], HAPPEX I – III [7–9], Mainz [10, 11], and G0 [12, 13], and remains a relevant consideration in experimental searches for BSM physics [14] and phenomena such as partonic charge symmetry breaking [15]. On the other hand, a number of theoretical studies, *e.g.*, [16–19], have proceeded in tandem with these experimental developments, including several global analyses of the elastic data [20–22].

It is also true that continued improvements in the technology of QCD global analyses of high energy data have inspired efforts to constrain the implications of nucleon strangeness for DIS PDFs such as the strange-antistrange momentum asymmetry [23]

$$xS^- = \int_0^1 dx x[s(x) - \bar{s}(x)] , \quad (1)$$

in which $s(x)$ and $\bar{s}(x)$ are PDFs for strange and antistrange quarks, respectively, carrying a fraction x of the nucleon’s momentum. Nonperturbative contributions to the strange PDFs have also been considered by various theoretical models [24–26], which are comparatively well-constrained by global analyses. Part of the interest in higher energy QCD processes extends to recent LHC measurements of neutral- and charge-current mechanisms [27] that are potentially sensitive to the quark density of the nucleon, though these are typically restricted to small x . At more intermediate kinematics, recent efforts to extract the strange PDFs from the semi-inclusive production of K^\pm [28] have also been made, though such undertakings present the added difficulty of model dependence associated with the required nonperturbative fragmentation functions.

Although PV DIS and elastic scattering analyses would seem to represent different aspects of the same essential phenomenology, to our knowledge they have not yet been systematically treated using a common framework. One such approach that facilitates the simultaneous computation of elastic form factors and DIS observables is a Fock expansion of the nucleon wave function into states explicitly involving strange and antistrange quarks, as might be carried out on the light front [29].

We organize our paper as follows: in Sec. II we present the basic details of our light-front model and use it to find expressions for the strangeness contributions to the vector form factors of the nucleon. In Sec. III, we use the light-front wave functions of Sec. II to determine expressions for the PDFs $s(x)$ and $\bar{s}(x)$, and observe that existing information from QCD global analyses of these objects impose constraints upon the parameters of the light-front wave functions. In Sec. IV, we consider the implications of these DIS constraints for elastic observables, and conclude in Sec. V.

II. LIGHT-FRONT FORMALISM

To evaluate the strangeness contributions to the nucleon Sachs form factors, we base our formalism upon a 2-body Fock state expansion of the nucleon wave function. In full generality, the n -particle light-front wave function for an initial-state proton of mass M and 4-momentum $P^\mu = (P^+, \mathbf{P}_\perp, P^-)$ [29] can be expanded as

$$\begin{aligned} |\Psi_P^\lambda(P^+, \mathbf{P}_\perp)\rangle &= \frac{1}{16\pi^3} \sum_n \prod_{i=1}^n \int \frac{dx_i d^2\mathbf{k}_{\perp i}}{\sqrt{x_i}} 16\pi^3 \delta\left(1 - \sum_{i=1}^n x_i\right) \delta^{(2)}\left(\sum_{i=1}^n \mathbf{k}_{\perp i}\right) \\ &\times \psi_n^\lambda(x_i, \mathbf{k}_{\perp i}, \lambda_i) |n; k_i^+, x_i \mathbf{P}_\perp + \mathbf{k}_{\perp i}, \lambda_i\rangle ; \end{aligned} \quad (2)$$

for the 2-body mechanism, physically associated with the process whereby the proton fluctuates into a state consisting of, *e.g.*, a virtual strange quark and a tetraquark spectator (made up of the usual $[uud]$ valence content of the proton and virtual \bar{s} , though for generality we leave the formalism independent of the struck quark flavor at this stage). We select $n = 2$ and obtain

$$|\Psi_P^\lambda(P^+, \mathbf{P}_\perp)\rangle = \frac{1}{16\pi^3} \sum_{q=s,\bar{s}} \int \frac{dx d^2\mathbf{k}_\perp}{\sqrt{x(1-x)}} \psi_{q\lambda_q}^\lambda(x, \mathbf{k}_\perp) |q; xP^+, x\mathbf{P}_\perp + \mathbf{k}_\perp\rangle, \quad (3)$$

following a trivial integration over dx_2 , $d^2\mathbf{k}_{\perp 2}$, and setting $x := x_1$. Note that in Eqs. (2) – (3) λ , λ_q refer to the helicity of the initial proton and struck quark, respectively, and as usual the light-front momentum fraction is $x = k^+/P^+$ of the intermediate quark (k) with respect to the parent nucleon (P). In particular, the object $\psi_{(q=s,\bar{s})\lambda_q}^\lambda$ represents the light-front wave function (LFWF) describing the amplitude for the proton to dissociate into an intermediate state involving a spin-1/2 strange or antistrange quark and scalar tetraquark spectator. The requirements of the Pauli principle are maintained through our use of the Fock expansion of Eq. (2), and we also assume that the two 5-quark states corresponding to the struck quark and antiquark are orthogonal.

Thus, using the standard definition of the electromagnetic current in terms of Dirac/Pauli operators between nucleonic states

$$\langle P', \lambda' | J_{EM}^\mu | P, \lambda \rangle = \bar{u}_{\lambda'}(P') \left\{ \gamma^\mu F_1(Q^2) + i \frac{\sigma^{\mu\nu} q_\nu}{2M} F_2(Q^2) \right\} u_\lambda(P), \quad (4)$$

where here and in the following, primed quantities apply to the final state, we can access the elastic form factors $F_{1,2}(Q^2)$ by computing matrix elements of the $\mu = +$ components of the current operators of Eq. (4) in a basis defined by the appropriate proton helicity combinations. Namely,

$$\begin{aligned} F_1(Q^2) &= \frac{1}{2P^+} \langle P', \lambda' = +1 | J_{EM}^+ | P, \lambda = +1 \rangle, \\ F_2(Q^2) &= \frac{2M}{[q^1 + iq^2]} \frac{1}{2P^+} \langle P', \lambda' = -1 | J_{EM}^+ | P, \lambda = +1 \rangle, \end{aligned} \quad (5)$$

where for the states $|P, \lambda\rangle$, we make use of the expressions of Eq. (3). Substituting these, and noting the general normalization condition

$$\langle n; p_i^+, \mathbf{p}_{\perp i}, \lambda_i | n; p_i^+, \mathbf{p}_{\perp i}, \lambda_i \rangle = \prod_{i=1}^n 16\pi^3 p_i^+ \delta(p_i^+ - p_i^+) \delta^{(2)}(\mathbf{p}_{\perp i} - \mathbf{p}_{\perp i}) \delta_{\lambda_i \lambda_i} \quad (6)$$

to determine the quark state overlaps implicit in Eq. (5), one arrives at [30] the quark-specific contributions

$$\begin{aligned} F_1^q(Q^2) &= e_q \int \frac{dx d^2\mathbf{k}_\perp}{16\pi^3} \sum_{\lambda_q} \psi_{q\lambda_q}^{*\lambda=+1}(x, \mathbf{k}'_\perp) \psi_{q\lambda_q}^{\lambda=+1}(x, \mathbf{k}_\perp), \\ F_2^q(Q^2) &= e_q \frac{2M}{[q^1 + iq^2]} \int \frac{dx d^2\mathbf{k}_\perp}{16\pi^3} \sum_{\lambda_q} \psi_{q\lambda_q}^{*\lambda=-1}(x, \mathbf{k}'_\perp) \psi_{q\lambda_q}^{\lambda=+1}(x, \mathbf{k}_\perp), \end{aligned} \quad (7)$$

where q corresponds to s or \bar{s} and $e_s = -1/3$ and $e_{\bar{s}} = 1/3$. These equations are obtained because single-quark operators such as those originating in the electromagnetic current of Eq. (4) do not connect the two components of Eq. (3) under the model assumption that the two 5-quark states are orthogonal.

The spin structure of the dissociation $P \rightarrow q(\bar{q}) \oplus uud\bar{q}(q)$, in which the $uudq(\bar{q})$ tetraquark state is assumed to possess an overall scalar behavior, is encoded in the LFWFs $\psi_{q\lambda_q}^\lambda(x, \mathbf{k}_\perp)$. Again following Ref. [30], these can be specified up to a quark-level wave function, which we denote $\tilde{\psi}_q$ and constitutes the principal result of the present analysis:

$$\begin{aligned} \psi_{q\lambda_q=+1}^{\lambda=+1}(x, \mathbf{k}_\perp) &= \frac{1}{\sqrt{1-x}} \left(\frac{m_q}{x} + M \right) \tilde{\psi}_q, \\ \psi_{q\lambda_q=-1}^{\lambda=+1}(x, \mathbf{k}_\perp) &= \frac{-1}{\sqrt{1-x}} \frac{1}{x} (k^1 + ik^2) \tilde{\psi}_q, \\ \psi_{q\lambda_q=+1}^{\lambda=-1}(x, \mathbf{k}_\perp) &= \frac{1}{\sqrt{1-x}} \frac{1}{x} (k^1 - ik^2) \tilde{\psi}_q, \\ \psi_{q\lambda_q=-1}^{\lambda=-1}(x, \mathbf{k}_\perp) &= \frac{1}{\sqrt{1-x}} \left(\frac{m_q}{x} + M \right) \tilde{\psi}_q. \end{aligned} \quad (8)$$

Inserting these expressions into Eq. (7) provides the desired formulas for our light-front model of strangeness. Integrating over the light-front fraction x and \mathbf{k}_\perp , we are left with a description of the Q^2 dependence of $F_{1,2}^q(Q^2)$, namely,

$$F_1^q(Q^2) = \frac{e_q}{16\pi^2} \int \frac{dx dk_\perp^2}{x^2(1-x)} \left(k_\perp^2 + (m_q + xM)^2 - \frac{1}{4}(1-x)^2 Q^2 \right) \tilde{\psi}'_q \tilde{\psi}_q, \quad (9)$$

$$F_2^q(Q^2) = \frac{e_q M}{8\pi^2} \int \frac{dx dk_\perp^2}{x^2} (m_q + xM) \tilde{\psi}'_q \tilde{\psi}_q. \quad (10)$$

To treat these contributions in our framework, we complete our LFWFs for the intermediate production of (anti)quarks (including strange) by specifying the product $\tilde{\psi}'_q \tilde{\psi}_q$:

$$\begin{aligned} \tilde{\psi}'_q \tilde{\psi}_q &= \frac{N_q}{\Lambda_q^4} \exp(-s_q/\Lambda_q^2), \\ \tilde{\psi}'_{\bar{q}} \tilde{\psi}_{\bar{q}} &= \frac{N_{\bar{q}}}{\Lambda_{\bar{q}}^4} \exp(-s_{\bar{q}}/\Lambda_{\bar{q}}^2), \end{aligned} \quad (11)$$

in which $\Lambda_{q,\bar{q}}$ are cutoffs for the momentum integrals of Eqs. (9) – (10), and the factors of $\Lambda_{q,\bar{q}}^{-4}$ are included to ensure the dimensionlessness of the wave function normalization constants $N_{q,\bar{q}}$. Also, we take the Q^2 -dependent center-of-mass energy of the quark-spectator system to be

$$s_q = \frac{1}{x(1-x)} \left[k_\perp^2 + (1-x)m_q^2 + xm_{S_p}^2 + \frac{1}{4}(1-x)^2 Q^2 \right], \quad (12)$$

where $m_{S_p}^2$ is the squared mass of the 4-quark scalar spectator, and a similar expression holds for $s_{\bar{q}}$. For the sake of the forthcoming numerical analysis, we find it convenient to write $m_{S_p} = \alpha m_{S_p}$, such that the parameter α amounts to a measure of the mass-splitting of the spectator states. We thus take the basic expressions of our light-front model to be

$$F_1^q(Q^2) = \frac{e_q N_q}{16\pi^2 \Lambda_q^4} \int \frac{dx dk_\perp^2}{x^2(1-x)} \left(k_\perp^2 + (m_q + xM)^2 - \frac{1}{4}(1-x)^2 Q^2 \right) \exp(-s_q/\Lambda_q^2), \quad (13)$$

$$F_2^q(Q^2) = \frac{e_q N_q M}{8\pi^2 \Lambda_q^4} \int \frac{dx dk_\perp^2}{x^2} (m_q + xM) \exp(-s_q/\Lambda_q^2), \quad (14)$$

while the same expression with $q \rightarrow \bar{q}$ provides the description for elastic scattering from antiquarks.

In fact, the more compact expressions of Eqs. (12) – (14) have followed from definitions of the individual initial/final state wave functions; *i.e.*,

$$\begin{aligned} \tilde{\psi}_q &= \frac{\sqrt{N_q}}{\Lambda_q^2} \exp \left\{ -M_{0q}^2(x, \mathbf{k}_\perp, \mathbf{q}_\perp) / 2\Lambda_q^2 \right\}, \\ \tilde{\psi}'_q &= \frac{\sqrt{N_q}}{\Lambda_q^2} \exp \left\{ -M'_{0q}{}^2(x, \mathbf{k}_\perp, \mathbf{q}_\perp) / 2\Lambda_q^2 \right\}, \end{aligned} \quad (15)$$

where the initial and final state invariant masses can be written as [30]

$$\begin{aligned} M_{0q}^2(x, \mathbf{k}_\perp, \mathbf{q}_\perp) &= \frac{(\mathbf{k}_\perp - \frac{1}{2}(1-x)\mathbf{q}_\perp)^2 + m_q^2}{x} + \frac{(\mathbf{k}_\perp - \frac{1}{2}(1-x)\mathbf{q}_\perp)^2 + m_{S_p}^2}{1-x}, \\ M'_{0q}{}^2(x, \mathbf{k}_\perp, \mathbf{q}_\perp) &= \frac{(\mathbf{k}_\perp + \frac{1}{2}(1-x)\mathbf{q}_\perp)^2 + m_q^2}{x} + \frac{(\mathbf{k}_\perp + \frac{1}{2}(1-x)\mathbf{q}_\perp)^2 + m_{S_p}^2}{1-x}, \end{aligned} \quad (16)$$

and it is straightforward to show $s_q = (M_{0q}^2 + M'_{0q}{}^2)/2$, using the fact that $\mathbf{q}_\perp^2 = Q^2$.

The Gaussian wave function chosen to describe the nucleon-quark-spectator interaction in Eq. (11) is by no means unique, and other ground-state choices are well-motivated, particularly power-law expressions such as

$$\tilde{\psi}_q = \frac{\sqrt{N_q}/\Lambda_q^2}{\left(1 + M_{0q}^2/2\Lambda_q^2\right)^\gamma}, \quad \tilde{\psi}'_q = \frac{\sqrt{N_q}/\Lambda_q^2}{\left(1 + M'_{0q}{}^2/2\Lambda_q^2\right)^\gamma}, \quad (17)$$

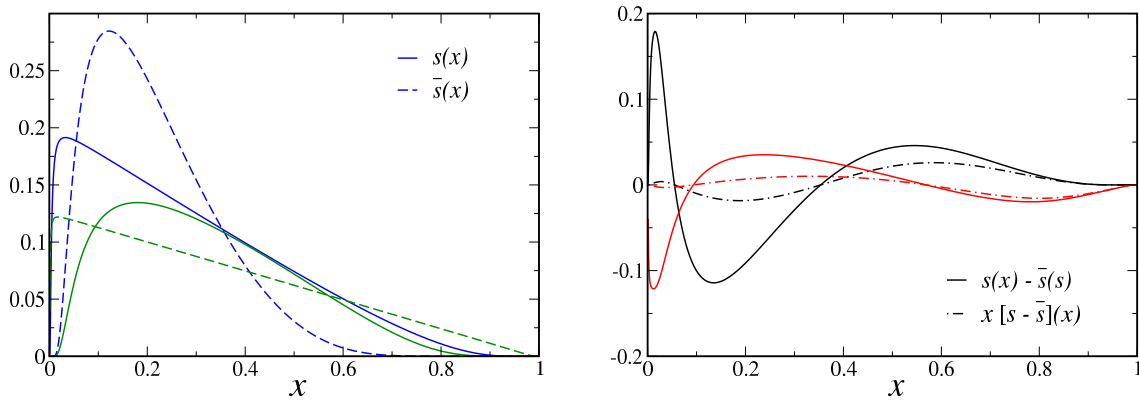


FIG. 1. (Left) We plot predictions for $s(x)$ [solid curves] and $\bar{s}(x)$ [dashed lines] using the model wave functions G1 (blue) and G2 (green) defined by the numerical values of Table I in Eq. (21). (Right) The integrands of the sum rule $\int_0^1 dx [s(x) - \bar{s}(x)] = 0$ (solid) and of xS^- as given by Eq. (1). In this case, results computed with G1 and G2 are given by black and red curves, respectively.

in which the selection $\gamma = 2$ would specify a dipole-like model.

As indicated, Eqs. (13) – (14) also apply to antiquarks, and we therefore always compute the total contribution as

$$\begin{aligned}
 F_{1,2}^{q\bar{q}}(Q^2) &= F_{1,2}^q(Q^2) - F_{1,2}^{\bar{q}}(Q^2) \implies \\
 G_E^{q\bar{q}}(Q^2) &= F_1^{q\bar{q}}(Q^2) - \frac{Q^2}{4M^2} F_2^{q\bar{q}}(Q^2), \quad G_M^{q\bar{q}}(Q^2) = F_1^{q\bar{q}}(Q^2) + F_2^{q\bar{q}}(Q^2), \quad (18)
 \end{aligned}$$

where we have used the standard expressions to construct the familiar Sachs parametrization in the second line, and we take $q = s$ for the strange components in the remainder of this analysis. The strangeness contributions to the latter quantities of Eq. (18) are in fact what have typically been extracted in experimental efforts, and there has been a dedicated drive to measure them at a range of facilities via Rosenbluth-separated electron-nucleon elastic scattering. In particular, the Sachs form factors of Eq. (18) are defined such that the nucleon's strange magnetic moment and charge radius follow from the limits

$$\begin{aligned}
 \mu_s &= G_M^{s\bar{s}}(Q^2 = 0), \\
 \rho_s &= -6 \left. \frac{dG_E^{s\bar{s}}(Q^2)}{dQ^2} \right|_{Q^2=0}; \quad (19)
 \end{aligned}$$

we shall consider their behavior as well as $G_{E,M}^{s\bar{s}}(Q^2)$ in Sec. IV after a discussion of the role played by DIS.

III. DEEPLY INELASTIC SCATTERING AND PDFS

An important element of the current framework is the total magnitude of the strangeness wave function — calculable from the LFWFs given in Eq. (11); this may be taken from the quantity

$$P_s := -3 F_1^s(Q^2 = 0) \equiv 3 F_1^{\bar{s}}(Q^2 = 0), \quad (20)$$

which amounts to the total multiplicity of strange quarks in the nucleon, and may serve as a constraint in applying the preceding formalism to predictions of $G_{E,M}^{s\bar{s}}$. The factors of ∓ 3 are necessary due to the fact that Eq. (20) is directly related to the probabilistic quark-level PDFs, which do not involve explicit factors of the struck quark charge, unlike the vector form factors of Eq. (7). Otherwise, $F_1^s(Q^2 = 0)$ may be evaluated using the definition given in Eq. (13).

Actually, the framework embodied by Eq. (13) lends itself to the computation of quark distributions for strangeness in the nucleon. We use the wave function model of the previous section to compute the strangeness distributions as

$$\begin{aligned}
 s(x) &= \frac{N_s}{16\pi^2 \Lambda_s^4} \int \frac{dk_\perp^2}{x^2(1-x)} \left(k_\perp^2 + (m_s + xM)^2 \right) \exp(-s_s/\Lambda_s^2), \\
 \bar{s}(x) &= \frac{N_{\bar{s}}}{16\pi^2 \Lambda_{\bar{s}}^4} \int \frac{dk_\perp^2}{x^2(1-x)} \left(k_\perp^2 + (m_{\bar{s}} + xM)^2 \right) \exp(-s_{\bar{s}}/\Lambda_{\bar{s}}^2), \quad (21)
 \end{aligned}$$

and the invariant mass s_s of the system involving the strange quark is given by Eq. (12). Hence, the probability distributions $s(x)$, $\bar{s}(x)$ go like the x -unintegrated form factor $F_1^{s\bar{s}}(Q^2 = 0)$. We note the similarity of the spin-structure evident in Eq. (21) to the quark-diquark distributions derived in previous models of other flavor sectors [31, 32].

Using the expressions of Eq. (21), we can compute the strangeness asymmetry defined in Eq. (1), as well as the related total momentum carried by the strange sea,

$$xS^+ = \int_0^1 dx x[s(x) + \bar{s}(x)] , \quad (22)$$

both of which have been the subject of DIS global analyses [23]. As an illustrative example, the CTEQ collaboration has estimated constraints to both xS^- and xS^+ using the world's data (at the time of CTEQ6.5S) for various high energy QCD processes [33]. Doing so, they obtained the bounds

$$0.018 \leq xS^+ \leq 0.040 , \quad -0.001 \leq xS^- \leq 0.005 , \quad (23)$$

which must serve as an important bound upon any model based on Eqs. (13) – (14). Although various other determinations of xS^\pm exist [23], the uncertainties about $xS^\pm \sim 0$ are typically comparable to the CTEQ6.5S values of Eq. (23), and we proceed with these without loss of generality.

TABLE I. Parameter values yielding the greatest spread in μ_s , ρ_s consistent with the CTEQ6.5S limits of Eq. (23). Masses and cutoffs are given in units of [GeV], while $N_{s,\bar{s}}$ are strictly dimensionless. Parameter combinations labeled *G1*, *G2* make use of the Gaussian wave functions of Eq. (11), while *P1*, *P2* follow from the power law expression in Eq. (17) with $\gamma = 2$.

model	xS^+	xS^-	N_s	$N_{\bar{s}}$	Λ_s	$\Lambda_{\bar{s}}$	m_{S_p}	α	P_s	μ_s	ρ_s^D
G1	0.040	0.005	46.54	1143.	4.75	1.25	3.0	0.7	8.05%	0.035	-0.137
G2	0.040	-0.001	56.44	20.22	1.25	8.25	1.18	1.3	6.16%	-0.024	0.081
P1	0.040	0.005	40.6	507.	8.25	1.25	1.96	1.3	7.13%	0.016	-0.038
P2	0.040	-0.001	120.	35.5	1.25	3.0	1.44	1.3	6.72%	-0.018	0.068

We therefore incorporate these DIS constraints upon xS^\pm by scanning the available parameter space of the LFWF model outlined in Sec. II, admitting only those input combinations that are consistent with the bounds of Eq. (23). Both formal constraints and model assumptions reduce the possible eight free parameters of our framework — $m_{s,\bar{s}}$, $N_{s,\bar{s}}$, $\Lambda_{s,\bar{s}}$, m_{S_p} , and α — to a set of five independent model inputs. In the present analysis, we assume a fixed constituent mass for the struck quark, such that for strange, $m_{s,\bar{s}} = 0.4$ GeV. Fundamental properties of the form factors themselves enable us to make an additional reduction. Due to the requirement of zero net strangeness in the nucleon, $G_E^{s\bar{s}}(Q^2 = 0) \equiv 0$ [essentially equivalent to the DIS condition $\int_0^1 dx[s(x) - \bar{s}(x)] = 0$], and we may then determine a simple relation between $N_s \sim N_{\bar{s}}$, the latter of which we tabulate together with the model input parameters in Table I. The remaining model space is scanned by assigning plausible ranges to input parameters and sampling the allowed values within the resulting interval according to a defined frequency (typically, 10 points). In general, we restrict $1.25 \leq \Lambda_{s,\bar{s}} \leq 10$ GeV, $m_s \leq m_{S_p} \leq 3$ GeV, and $\alpha = 1 \pm 50\%$. We point out also that the lower bounds $\Lambda_{s,\bar{s}}$ are chosen to avoid numerical instabilities that can occur if the wave function cutoff scales are allowed to venture too far below the nucleon mass.

We proceed by using the Gaussian formulation of Eqs. (11) – (14) and finding combinations of the CTEQ6.5S bounds of Eq. (23) responsible for the widest spread in the elastic observables μ_s and ρ_s introduced in Eq. (19). Then, if we take the Gaussian calculation constrained to satisfy the combination of extrema [$xS^+ = 0.040$, $xS^- = 0.005$] (G1) and [$xS^+ = 0.040$, $xS^- = -0.001$] (G2) as distinct models, we obtain the family of parameter values listed in Table I after running scans over the input parameter ranges just described with a 50 point sampling of $1 \leq N_s \leq 100$. Using these in the expressions of Eq. (21), we plot in the left panel of Fig. 1 examples for the behavior of $s(x)$ [solid curves] and $\bar{s}(x)$ [dashed curves] for fits corresponding to G1 [in blue], and G2 [in green]. Moreover, the integrands of the moment defined by Eq. (1), as well as for the first moment $\int_0^1 dx[s(x) - \bar{s}(x)] = 0$, are plotted in the right hand side of Fig. 1, with the latter given by solid and the former by dot-dashed curves, respectively. In this case, the result of using the G1 wave functions are given in black, whereas the calculation with the G2 wave function corresponds to the red lines, and the expected behavior that the first moment of $s(x) - \bar{s}(x)$ vanishes is recovered. While the difference in shapes among the quark distributions of Fig. 1 is striking, it should be kept in mind that these represent bounds on the parameter space for the LFWFs and hence are extremal choices yielding the greatest spread in μ_s , ρ_s consistent with the DIS constraints of Eq. (23).

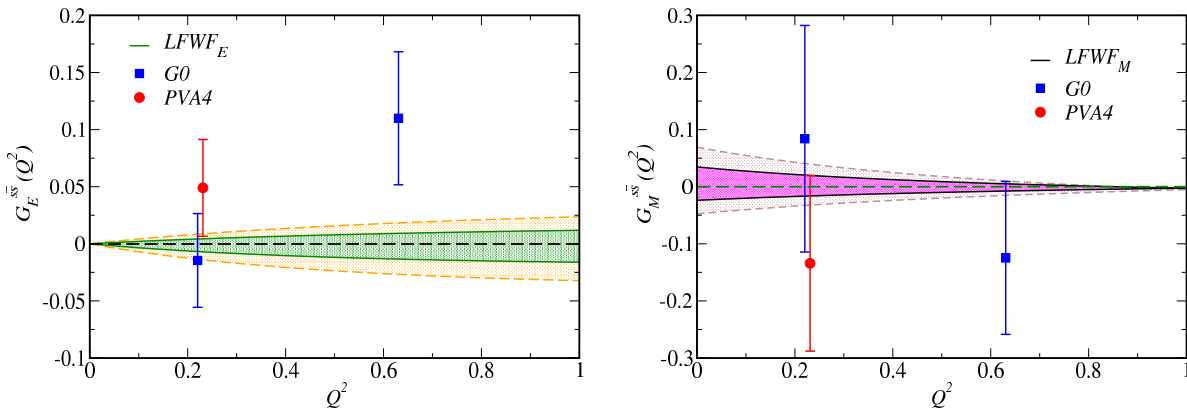


FIG. 2. A comparison of the systematic LFWF uncertainty between the Gaussian models G1 and G2 against Rosenbluth-separated measurements for $G_E^{s\bar{s}}(Q^2)$ (left) and $G_M^{s\bar{s}}(Q^2)$ (right). The inner bands represent the constraints due to CTEQ6.5S, while the outer bands correspond to *ad hoc* bounds for xS^\pm produced by doubling the ranges of Eq. (23) so as to be more comparable to the experimental uncertainties of the elastic data.

We note also that the values of xS^\pm of Eq. (23) reported by CTEQ6.5S hold at the charm threshold $Q^2 = 1.69 \text{ GeV}^2 \sim m_c^2$, which represents a momentum scale slightly larger than would be natural to ascribe the nonperturbative strange model prediction of Eqs. (21). As such, if we instead applied the model distributions of Eqs. (21) to a somewhat lower initial scale $Q_0^2 < m_c^2$, QCD evolution would alter the magnitudes of the moments in xS^\pm as one moves to higher Q^2 . For example, to leading order (LO) in α_s , one has for the n^{th} moments $M_{\text{NS}}^n(Q^2)$ of non-singlet quark density combinations like xS^- [34]

$$M_{\text{NS}}^n(Q^2) = \left(\frac{\alpha_s(Q^2)}{\alpha_s(Q_0^2)} \right)^{\gamma_{\text{NS}}^{(\text{LO}),n}/2\beta_0} \cdot M_{\text{NS}}^n(Q_0^2) \implies M_{\text{NS}}^n(Q^2) \approx \left(\frac{\alpha_s(Q^2)}{\alpha_s(Q_0^2)} \right)^{0.41} \cdot M_{\text{NS}}^n(Q_0^2), \quad (24)$$

where the second relation follows from assuming $n_f = 3 - 4$ active flavors, and a more complicated behavior applies to singlet quantities like xS^+ . Thus, if one uses successively smaller starting scales Q_0^2 , larger and larger corrections to xS^- due to evolution are possible, but the reliability of a LO computation becomes more questionable. Either way, the result of Eq. (24) implies that the bounds for xS^- of Eq. (23) at $Q^2 = m_c^2$ would be a slight underestimate of the corresponding range at a lower scale $Q_0^2 \sim 1 \text{ GeV}^2$, but the systematic effect in our subsequent predictions should be small.

IV. ELASTIC SCATTERING AND STRANGE FORM FACTORS

Having constrained our Gaussian LFWF model according to the DIS global analyses, we may confront our results with some of the more recent data for $G_{E,M}^{s\bar{s}}(Q^2)$ — especially newer values from G0 and PVA4, as shown in Fig. 2.

Aside from precise measurements of the Sachs form factors, great interest attaches also to the parameters μ_s and ρ_s defined in Eq. (19), which have in fact already been constrained to some extent by previous analyses [21, 22], though the uncertainties of fits to elastic data remain fairly large. These fits generically proceed by ascribing a simple Q^2 dependence to the the vector and axial form factors, and leaving ρ_s and μ_s , as well as vector and axial masses as free parameters to be constrained by data. It is crucial to note, however, that the definition of ρ_s specified by Eq. (19) is not universal. In fact, the analysis contained in Ref. [35] explicitly accounts for the treatment of ρ_s as it appears in [21, 22], with the strangeness radius defined via

$$\rho_s^D := \left. \frac{dG_E^{s\bar{s}}}{d\tau} \right|_{\tau=0}, \quad \tau := Q^2/4M^2, \quad (25)$$

from which we conclude the relation between the definition of ρ_s according to Eq. (19) and that of the recent elastic global analyses [21, 22] to be

$$\rho_s \equiv -\frac{3}{2M^2} \rho_s^D. \quad (26)$$

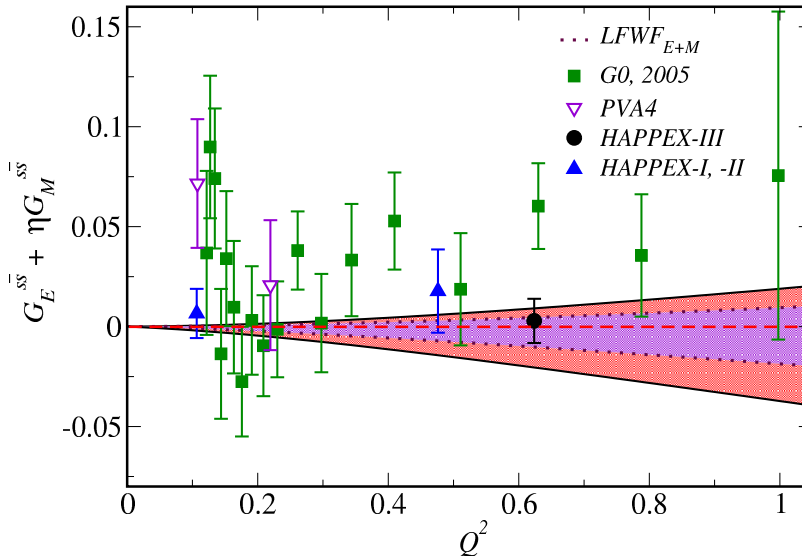


FIG. 3. An extension of the curves evaluated in Fig. 2 to the quantity $G_E^{s\bar{s}}(Q^2) + \eta G_M^{s\bar{s}}(Q^2)$ determined at forward kinematics. The colored bands about $G_E^{s\bar{s}}(Q^2) + \eta G_M^{s\bar{s}}(Q^2)$ are as described for Fig. 2.

For the sake of comparison, we shall refer to ρ_s^D (as we have reported in Table I). On the other hand, the dimensionless ‘magneton’ units of μ_s are generally standard across former calculations, and similarly match what we use here.

The LFWFs that gave rise to the quark distributions plotted in Fig. 1 may be used to compute $G_{E,M}^{s\bar{s}}(Q^2)$ using the exclusive formalism built in Sec. II. In Fig. 2 we compare our calculated $G_{E,M}^{s\bar{s}}(Q^2)$ with the separated data obtained by the G0 and Mainz collaborations; as explained, the plotted bands follow from scanning the five-dimensional parameter space spanned by N_s , $\Lambda_{s/\bar{s}}$, m_{S_p} , and α and selecting those combinations that yield wave functions sufficiently near the required values of xS^\pm (in this case, within $\sim 1\%$). Using wave functions computed with the parameter combinations labeled G1, G2 in Table I then generates the narrow inner bands plotted in Fig. 2, with the experimental uncertainties for the Rosenbluth-separated $G_{E,M}^{s\bar{s}}(Q^2)$ far outstripping the stringent bounds enforced by the CTEQ6.5S analysis of the DIS distributions. It must be pointed out that this behavior occurs systematically, and does not depend qualitatively upon the specific wave function used in Eq. (11); for example, the same essential procedure but with the dipole expressions of Eq. (17) [choosing $\gamma = 2$] and 5 point samplings of $1 < N_s < 200$ as well as the previously mentioned parameter ranges leads to a similar conclusion: the tight constraints to xS^\pm are such that any reasonable LFWF that generates consistent strangeness PDFs will predict values of μ_s , ρ_s that lie well within the reported errors of the elastic data plotted in Fig. 2. We summarize our numerical results with this scheme in the latter rows ‘P1, P2’ of Table I, but otherwise continue the remainder of the analysis with Eq. (11).

One might ask what level for xS^\pm is required for the width of the systematic model bands of Fig. 2 to begin to approximate the current experimental precision for $G_{E,M}^{s\bar{s}}$. This information is represented by the somewhat broader outer bands plotted in the same figure, which result from a similar calculation using bounds for xS^\pm that we increase by a factor of 2. Namely, the broad, outer bands of Figs. 2 – 3 follow from constraining scans to

$$xS^+ = 0.080 (\pm 1\%), \quad -0.002 \leq xS^- \leq 0.010, \quad (27)$$

i.e., a total strange momentum enhanced by a factor of 2 to $xS^+ = 0.080$, corresponding to a strange probability of $\sim 15\%$, and within an error about $xS^- = 0$ that we have also broadened by a factor of 2 with respect to the bounds of Eq. (23). That is, the simple result of this *ad hoc* increase to the bounds of xS^\pm is a doubling of the predictions for $G_{E,M}^{s\bar{s}}$ relative to the G1, G2 calculations using the parameters given in Table I.

The results of Fig. 2 may also be rendered in the combination measured by forward elastic experiments $G_E^{s\bar{s}}(Q^2) + \eta G_M^{s\bar{s}}(Q^2)$ using a trivial description of the Q^2 dependence of $\eta(Q^2) \sim 0.94 \cdot Q^2$, which is defined as the ratio of electromagnetic form factors $\eta = \tau G_M^\gamma / \epsilon G_E^\gamma$, with τ given in Eq. (25) and ϵ a kinematical parameter dependent upon the angle of the scattered electron. This is shown explicitly in Fig. 3 against forward form factor data obtained by G0 (as well as LVA4, and HAPPEX I–III). As with Fig. 2, the Gaussian models G1, G2 deviate from zero by margins that are generally well-exceeded by the uncertainties of the existing data.

We also compute the total strangeness probability according to Eq. (20), finding $P_s \sim 6 - 8\%$ with the models G1, G2 across the range determined by the CTEQ6.5S limits to xS^\pm . On the other hand, the artificially enhanced bands intended to rise onto the elastic error bars correspond to a still larger probability $P_s \sim 15\%$, as mentioned. That light-front models associated with strangeness probabilities of these magnitudes predict such small effects for $G_{E,M}^{s\bar{s}}$ is illustrative of the strength of the DIS constraints of Eq. (23).

Lastly, for the strangeness parameters μ_s and ρ_s^D given according to the conventions of Eq. (25), we find the range tolerated by the DIS bounds on xS^\pm to be significantly reduced relative to the values obtained from global fits to the existing elastic data:

$$-0.024 \leq \mu_s \leq 0.035, \quad -0.137 \leq \rho_s^D \leq 0.081. \quad (28)$$

We compare these values to the much larger ranges allowed by the recent fits of Ref. [22] in Table II. Also, these values are considerably smaller than the ranges one might determine from direct fits of the LFWF framework of Sec. II to the experimental data shown in Figs. 2 – 3, further underlining the force of the DIS limits beyond the precision of elastic measurements and urging improvements to the latter from future experiments.

TABLE II. We compare computed bounds for μ_s, ρ_s^D obtained by a recent global analysis of elastic scattering data [22] with the results of our calculation using the Gaussian LFWFs G1, G2 constrained by the CTEQ6.5S bounds to xS^\pm of Eq. (23).

	Ref. [22]	this analysis
μ_s range	$-0.52 \leq \mu_s \leq 0$	$-0.024 \leq \mu_s \leq 0.035$
ρ_s^D range	$0.34 \leq \rho_s^D \leq 1.5$	$-0.137 \leq \rho_s^D \leq 0.081$

V. CONCLUSION

We have developed a simple spinor-scalar model to decompose the nucleon wave function and gauge the potential contributions from the strange sector to elastic observables of the proton, particularly its strange charge radius and magnetic moment ρ_s and μ_s , respectively. In so doing, we have formulated wave functions of sufficient generality as to enable the computation of both DIS distribution functions as well as elastic scattering matrix elements, and we can therefore compute the strange Sachs form factors of the nucleon $G_{E,M}^{s\bar{s}}(Q^2)$ in a fashion that incorporates constraints from QCD global analyses of the strange PDF combinations xS^\pm given by Eqs. (1) and (22). Taking a representative DIS analysis [33] and a Gaussian expression for the strange quark-nucleon interaction as in Eq. (11) [though other forms such as Eq. (17) yield very similar results], we find the DIS limits to xS^\pm imply the tight bounds to μ_s and ρ_s^D reported in Eq. (28) and Table II. These parameter ranges are notably smaller than the results of global analyses based directly upon the available elastic data [20–22], with the clear suggestion being that if ground-state LFWFs are to be taken seriously, the current precision in elastic data is not yet adequate to be unambiguously sensitive to nucleon strangeness. Moreover, as the difference between our computed range in Eq. (28) and the results of, *e.g.*, [22] is roughly order-of-magnitude, further experimental investigation with enhanced precision will prove vital.

This reality is something of a double-edged sword, and the comparative smallness of the nucleon strangeness suggested by our results should simplify extractions of $\sin^2 \theta_W$; thus, one might conclude BSM physics searches based upon parity-violating electron scattering are relatively free of the potential “contamination” that might originate in backgrounds associated with the nucleon’s strange content.

The formalism presented here is intended to represent a simple approximation of the ground-state structure of the nucleon, and one might readily conceive various embellishments that more ably capture the relevant dynamics, including more elaborate wave functions involving additional spin structures — though these would presumably require additional input parameters. We also note that other observables of interest like the nucleon’s strange axial form factor $G_A^{s\bar{s}}(Q^2)$ and the lattice-calculable correlator $\langle N|\bar{s}s|N \rangle$ have not been treated in the present analysis.

ACKNOWLEDGMENTS

The work of TJH and GAM was supported by the U.S. Department of Energy Office of Science, Office of Basic Energy Sciences program under Award Number DE-FG02-97ER-41014. The work of MA was supported by the

Research in Undergraduate Institutions Program of the National Science Foundation under Grant No. 1205686.

- [1] M. Gell-Mann, Phys. Lett. **8**, 214 (1964).
- [2] J. D. Bjorken and S. L. Glashow, Phys. Lett. **11**, 255 (1964).
- [3] J. Ashman *et al.* [European Muon Collaboration], Phys. Lett. B **206**, 364 (1988).
- [4] D. B. Kaplan and A. Manohar, Nucl. Phys. B **310**, 527 (1988).
- [5] D. S. Armstrong and R. D. McKeown, Ann. Rev. Nucl. Part. Sci. **62**, 337 (2012) [arXiv:1207.5238 [nucl-ex]].
- [6] D. T. Spayde *et al.* [SAMPLE Collaboration], Phys. Rev. Lett. **84**, 1106 (2000) [nucl-ex/9909010].
- [7] K. A. Aniol *et al.* [HAPPEX Collaboration], Phys. Rev. C **69**, 065501 (2004) [nucl-ex/0402004].
- [8] K. A. Aniol *et al.* [HAPPEX Collaboration], Phys. Lett. B **635**, 275 (2006) [nucl-ex/0506011].
- [9] Z. Ahmed *et al.* [HAPPEX Collaboration], Phys. Rev. Lett. **108**, 102001 (2012) [arXiv:1107.0913 [nucl-ex]].
- [10] F. E. Maas *et al.* [A4 Collaboration], Phys. Rev. Lett. **93**, 022002 (2004) [nucl-ex/0401019].
- [11] F. E. Maas, K. Aulenbacher, S. Baunack, L. Capozza, J. Diefenbach, B. Glaser, T. Hammel and D. von Harrach *et al.*, Phys. Rev. Lett. **94**, 152001 (2005) [nucl-ex/0412030].
- [12] D. S. Armstrong *et al.* [G0 Collaboration], Phys. Rev. Lett. **95**, 092001 (2005) [nucl-ex/0506021].
- [13] D. Androic *et al.* [G0 Collaboration], Phys. Rev. Lett. **104**, 012001 (2010) [arXiv:0909.5107 [nucl-ex]].
- [14] D. Androic *et al.* [Qweak Collaboration], Phys. Rev. Lett. **111**, no. 14, 141803 (2013) [arXiv:1307.5275 [nucl-ex]].
- [15] M. Wagman and G. A. Miller, Phys. Rev. C **89**, 065206 (2014) [arXiv:1402.7169 [nucl-th]].
- [16] D. H. Beck and B. R. Holstein, Int. J. Mod. Phys. E **10**, 1 (2001) [hep-ph/0102053].
- [17] D. B. Leinweber, S. Boinepalli, A. W. Thomas, P. Wang, A. G. Williams, R. D. Young, J. M. Zanotti and J. B. Zhang, Phys. Rev. Lett. **97**, 022001 (2006) [hep-lat/0601025].
- [18] P. Wang, D. B. Leinweber and A. W. Thomas, Phys. Rev. D **89**, no. 3, 033008 (2014).
- [19] M. J. Iqbal and G. A. Miller, Phys. Rev. D **41**, 2817 (1990).
- [20] R. D. Young, J. Roche, R. D. Carlini and A. W. Thomas, Phys. Rev. Lett. **97**, 102002 (2006) [nucl-ex/0604010].
- [21] R. González-Jiménez, J. A. Caballero and T. W. Donnelly, Phys. Rept. **524**, 1 (2013) [arXiv:1111.6918 [nucl-th]].
- [22] O. Moreno, T. W. Donnelly, R. González-Jiménez and J. A. Caballero, arXiv:1408.3511 [nucl-th].
- [23] W. Bentz, I. C. Cloet, J. T. Londergan and A. W. Thomas, Phys. Lett. B **693**, 462 (2010) [arXiv:0908.3198 [nucl-th]].
- [24] A. I. Signal and A. W. Thomas, Phys. Lett. B **191**, 205 (1987).
- [25] S. J. Brodsky and B. Q. Ma, Phys. Lett. B **381**, 317 (1996) [hep-ph/9604393].
- [26] W. C. Chang and J. C. Peng, Phys. Rev. Lett. **106**, 252002 (2011) [arXiv:1105.2381 [hep-ph]].
- [27] G. Aad *et al.* [ATLAS Collaboration], Phys. Rev. Lett. **109**, 012001 (2012) [arXiv:1203.4051 [hep-ex]].
- [28] A. Airapetian *et al.* [HERMES Collaboration], Phys. Rev. D **89**, 097101 (2014) [arXiv:1312.7028 [hep-ex]].
- [29] S. J. Brodsky, D. S. Hwang, B. Q. Ma and I. Schmidt, Nucl. Phys. B **593**, 311 (2001) [hep-th/0003082].
- [30] I. C. Cloet and G. A. Miller, Phys. Rev. C **86**, 015208 (2012) [arXiv:1204.4422 [nucl-th]].
- [31] H. Meyer and P. J. Mulders, Nucl. Phys. A **528**, 589 (1991).
- [32] T. J. Hobbs, J. T. Londergan and W. Melnitchouk, Phys. Rev. D **89**, 074008 (2014) [arXiv:1311.1578 [hep-ph]].
- [33] H. L. Lai, P. M. Nadolsky, J. Pumplin, D. Stump, W. K. Tung and C.-P. Yuan, JHEP **0704**, 089 (2007) [hep-ph/0702268].
- [34] E. G. Floratos, D. A. Ross and C. T. Sachrajda, Nucl. Phys. B **129**, 66 (1977) [Erratum-ibid. B **139**, 545 (1978)].
- [35] M. J. Musolf, T. W. Donnelly, J. Dubach, S. J. Pollock, S. Kowalski and E. J. Beise, Phys. Rept. **239**, 1 (1994).